ROBUST AERODYNAMIC OPTIMIZATION STRATEGIES FOR ROTOR BLADE MORPHING AIRFOILS

F.Fusi*, P. M. Congedo, A. Guardone*, G. Quaranta***

*Dipartimento di Scienze e Tecnologie Aerospaziali – Politecnico di Milano
Campus Bovisa, Via La Masa 34, 20156 Milano – Italy
**Team CARDAMOM – INRIA Bordeaux Sud-Ouest
200 Avenue de la Vieille Tour, 33405 Talence Cedex – France
e-mail: francesca.fusi@polimi.it

Abstract

An aerodynamic optimization method is developed to define robust shapes for morphing airfoils for helicopter blades. The morphing strategy consists of a conformable camber airfoil which changes over the period of rotation of the blade to cope with the variable flow conditions encountered in forward flight. A robust or uncertainty-based approach is used to compute a reliable morphing airfoil, providing a low variance with respect to uncertainty affecting the operating conditions. In order to assess the effectiveness of the robust method, several optimization problems are performed, from a classical two-point drag minimization with lift coefficient constraint to a robust morphing camber optimization. The results of the optimization problems are compared and discussed to highlight the features of the robust approach.

1 INTRODUCTION

Helicopter rotor blades present a real challenge to aerodynamic design. In fact, rotor blades are required to operate with satisfactory performance in extremely different conditions, depending on the azimuthal position and the advance ratio, and good performance in one condition does not transfer to another one. A trade-off solution must be pursued, whose performance in each condition over the flight envelope is sub-optimal. A very attractive solution to this problem is the employment of a blade capable of changing its shape during flight, that is a morphing blade. Morphing rotor design is a challenging and active area of research [1]: recent studies have focused on conformable airfoils to reduce vibration [2] or postpone dynamic stall onset [3]. Because morphing structures typically imply increased weight, complexity and cost, an in-depth assessment of the potential aerodynamic benefit of such an approach is strongly recommended [4].

Additionally, the flow conditions encountered by rotor blades may vary due to the effects of the blade dynamics and flexibility, as well as the interaction with vortices and wakes trailed from preceding blades. It follows that the flow conditions considered at the design stage for the definition of the optimal two-dimensional section are usually affected by uncertainty, not only because they are estimates of the actual condition, but also because modelling involves some level of approximation of the real flowfield. In such a context, taking into account the variability of the modelling parameters in the optimization procedure is a possible way to result in a more reliable optimal design. This is the goal of uncertainty-based optimization. Specifically, robust optimization seeks an optimal design that is minimally sensitive with respect to changes of the uncertain parameters that define the problem. The result is a robust design that maintains satisfactory performance also in off-design conditions. Few works consider uncertainty in the field of helicopter design [5, 6, 7]. In the application to morphing structures, a high level of uncertainty affects the modelling of the environmental conditions encountered by the airfoil, and therefore robustness becomes critical to define reliable design.

In this work, a robust aerodynamic optimization method is developed to define robust shapes for morphing airfoils. The morphing strategy consists of a conformable camber airfoil which changes over the period of rotation of the blade to cope with the variable flow conditions encountered in forward flight.

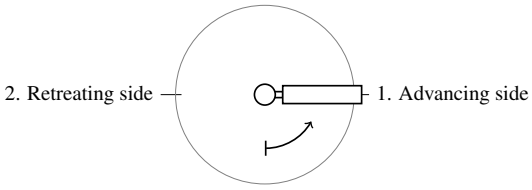

Figure 1: Scheme of operating conditions.

Because the employment of robust strategies is new to this application, an assessment of the performance of the robust optimization and the morphing strategy is presented. To this end several optimization problems are performed and compared, that may be categorised in the following types of optimization. The first kind is a "classical" airfoil optimization in forward flight condition, with a minimization of the drag coefficient subject to a target lift coefficient for trimming purposes. The second type is the robust optimization in forward flight condition, namely an optimization that seeks a shape with a lift-to-drag ratio robust against uncertain operating conditions. Finally, an aerodynamic optimization with a morphing camber airfoil is tackled. These optimization problems are described respectively in Sections 2, 3 and 4. Section 5 presents a comparison of the results of these problems.

2 FORWARD FLIGHT OPTIMIZATION

The optimization method presented in this work are developed to improve the aerodynamic performance of the airfoil for a rotor blade in forward flight conditions. Using a multi-point approach, two operating conditions are considered, i.e. advancing side and retreating side, the conditions encountered by a specific blade section at 90 and 270 degrees azimuth angles (see Fig. 1). In the former condition the rotor blade encounters transonic flow and low values of the angle of attack. In the latter, the angle of attack is typically high and the local Mach number is close to the incompressible limit. For the optimization problem tackled in this work, the operating conditions for advancing and retreating sides are taken from the Mach number–angle of attack cycle presented in Ref. [8, p.296] and they are reported in Tab. 1.

The optimization of helicopter rotor airfoil in forward flight consists typically in the minimization of the drag coefficient C_D ensuring the satisfaction of lift and moment constraints. Examples of such an approach are given in Refs. [9, 10, 11]. In this work, a target lift coefficient is set to consider a specific trim condition and the moment coefficient is bounded with a given threshold to avoid excessive loading on the blade structure. The minimization problem can be formulated as a multi-objective optimization. In fact, an optimal shape for the advancing side would be a thin, slightly cambered airfoil to postpone drag rise to higher Mach number values, whereas the optimal shape in the retreating side should adapt the camber to higher angle of attack, for instance with a nose-droop. In mathematical terms, the bi-objective optimization reads

$$\begin{aligned} \text{minimize:} \quad & (C_{D_1}(\boldsymbol{x}), C_{D_2}(\boldsymbol{x})) \\ \text{subject to:} \quad & C_{L_1}(\boldsymbol{x}) = \overline{C_{L_1}} \quad C_{M_1}(\boldsymbol{x}) \leq \overline{C_{M_1}} \\ & C_{L_2}(\boldsymbol{x}) = \overline{C_{L_2}} \quad C_{M_2}(\boldsymbol{x}) \leq \overline{C_{M_2}} \\ \text{by changing:} \quad & \boldsymbol{x} \end{aligned} \tag{1}$$

where $\boldsymbol{x}$ are the design variables. The subscript is used to indicate (1) the advancing side and (2) the retreating side. The values of the lift constraint $\overline{C_L}$ and moment constraint $\overline{C_M}$ are set for each side with the intent of producing a design that improves the performance of the NACA 23012 airfoil, a classical shape for helicopter rotors (see Tab. 2).

Case	α[deg]	M[-]	Re [-]
1.	-1.5	0.75	4.6e6
2.	12.5	0.28	1.7e6

Table 1: Operating conditions.

Case	$\overline{C_L}$	$\overline{C_M}$
1.	0.025	0.08
2.	1.411	0.04

Table 2: Lift and moment constraints.

2.1 Design variables

Particular attention is drawn to the design variables. First, to describe an airfoil shape with a finite set of variables, a shape parameterization is required. The airfoil shape is decomposed into the camber mean line and the thickness distribution, with the intent of changing the camber distribution over the blade rotation period, while holding the thickness distribution fixed. In fact, the morphing airfoil considered in the work is a conformable camber airfoil that changes with a 1/rev frequency to enhance the aerodynamic performance.

In particular, the camber mean line $\zeta_c(\psi)$ and the thickness distribution $\zeta_t(\psi)$, expressed as a function

of the chordwise coordinate divided by chord length ($\psi = x/c$), are obtained by means of a shape parameterization based on the Class/Shape function Transformation [12]. The parameterization is based on two functions: a geometry class function $C(\psi)$, which determines a group of geometries, and a shape function $S(\psi)$ that defines the specific shape of the geometry. The parameterization for the camber line and the thickness distribution reads

$$\begin{aligned} \zeta_c(\psi) &= C_c(\psi)\ S_c(\psi) \\ \zeta_t(\psi) &= C_t(\psi)\ S_t(\psi) \end{aligned} \tag{2}$$

where the subscript $_c$ and $_t$ refers to the camber and thickness respectively. With respect to the original formulation, the coordinate of the camber mean line and thickness at the trailing edge are set to zero to consider closed leading edge and zero geometric angle of attack. In addition, the class functions are defined as follows

$$C_c(\psi) = \psi(1-\psi) \qquad C_t(\psi) = \sqrt{\psi}(1-\psi). \tag{3}$$

While the class function for the thickness distribution is the one suggested in Ref. [12] to define a rounded nose distribution close to the leading edge, the class function for the camber presents a linear term to avoid vertical slope of the camber distribution at the leading edge.

The shape function $S(\psi)$ is given by a Bernstein polynomial of order n, whose coefficients represent the design variables $\boldsymbol{x}_s$ of the optimization problem. A convergence study, not reported here for brevity, suggested the employment of 4 design variables for each distributions that yield to 10 design variables. Finally, from the camber line and thickness distribution the upper surface ζ_u and lower surface ζ_l are obtained applying the thickness perpendicular to the camber line

$$\begin{aligned} \zeta_u &= \zeta_c + \zeta_t \cos(\theta) \\ \zeta_l &= \zeta_c - \zeta_t \cos(\theta), \end{aligned} \tag{4}$$

where $\theta = \arctan\left(\frac{\mathrm{d}\zeta_c}{\mathrm{d}\psi}\right)$. Please note that also the ψ coordinate of the resulting airfoil will be affected by this addition of vectors.

In addition to the coefficients describing the shape of the airfoil, the angle of attack can be regarded as a design variable. In fact, it is possible to solve the constrained optimization problem stated in Eq. (1) by acting on the airfoil design variables $\boldsymbol{x}_s$ to minimize the drag coefficient and on the angle of attack to track the target lift coefficient inside two nested loops. In this sense, each airfoil tested in the optimization loop is obtained with a specific set $\boldsymbol{x}_s$, and its performance are evaluated computing the angle of attack α that provides the desired lift coefficient. The nested optimization loops used to implement this procedure are better described in Sec. 2.3. Thus, the resulting set of design variables is $\boldsymbol{x} = \{\boldsymbol{x}_s, \alpha\}$.

2.2 Aerodynamic models

A model describing the aerodynamic load acting on the airfoil is necessary to compute the objective function of the optimization problem. The aerodynamic models used in this work are different for each side of the blade in order to capture the specific features of the flow in such different operating conditions, while limiting the computational effort.

In the advancing side, a numerical solver of the Euler equations is used, namely the Stanford University Unstructured (SU^2) software suite [13, 14]. The solver provides several space discretization schemes, among which the second-order Jameson-Schmidt-Turkel scheme is employed. An implicit Euler, local time-stepping is used to converge to the steady-state solution, and the GMRES method in conjunction with the LU SGS preconditioner is used to solve the resulting system. For this computation a two-dimensional coarse unstructured mesh of 20480 rectangular cells is used. Because the Euler equations are used, a contribution associated with viscous effects is added combining the van Driest II method and a form-factor correction as presented in Ref. [15].

In the retreating side featuring subsonic condition below the static stall boundary, the XFOIL code is adopted, which is an aerodynamic code with coupled panel and integral boundary layer methods developed for the analysis of subsonic, isolated airfoils [16]. This code is chosen because it provides a fast and sufficiently accurate estimation of the aerodynamic force coefficients for a two-dimensional section.

2.3 Optimization algorithm

To solve the optimization problem in Eq. (1) a multi-objective optimization algorithm is required. In this work, the Non-dominated Sorting Genetic Algorithm is chosen for its ability to explore the design space and to deal with multiple objectives. Inside the genetic algorithm loop, an inner loop is nested to deal with the lift coefficient constraint. In particular, for each design vector $\boldsymbol{x}_{s,k}$ of the k-th iteration in the genetic loop, a secant method is used to find the angle of attack α_k that guarantees $C_{L,k} = \overline{C_L}$. The method converges in a few iterations, owing to the linearity of the lift coefficient for most airfoils in the vicinity of the considered values of the angle of attack. Lack

of convergence within few iterations is not critical, because this happens for airfoils with poor values of the lift coefficient that should be discarded anyway. The result of the two nested loops is a set of optimal solutions defined by a design vector $\{\boldsymbol{x}_s, \alpha\}$.

3 ROBUST OPTIMIZATION

The objective of robust optimization is to design an airfoil that is minimally sensitive to the variation of the operating conditions. In this case, it is considered that the operating conditions at which the blade section will operate are affected by the uncertainty arising due to modelling assumptions of physical parameters necessary at the design stage.

Due to the uncertainty, the objective function f is no longer only a function of the design variables $\boldsymbol{x}$, but it also depends on the uncertain variables $\boldsymbol{\xi}$. If the uncertain variables are defined within a probabilistic framework, the objective function is a stochastic variable with a probability distribution function. Thus, the optimization problem has to define a measure of the variability of the function to be optimized. In robust design, the shape of the airfoil is sought to simultaneously optimize the mean value of the objective $\mu(f)$ and to minimize the variance $\sigma^2(f)$ of the objective function f, computed with respect to the uncertainties of the operating conditions. By minimizing the variance as well, the optimal shape results more reliable against variation of the design operating conditions.

Within this uncertain framework a minimization with a target lift coefficient in a specific design conditions loses its meaning. However, a robustly optimal airfoil with a satisfactory lift-to-drag ratio in a range of conditions could be used to trim the aircraft in a specific condition keeping always a low drag coefficient. In addition, if the robustness of the lift-to-drag ratio will translate into the drag coefficient at a specific target lift coefficient, a robust shape would ensure less variability of the required power due to aerodynamic drag.

In particular, for the problem under analysis, in the advancing side the lift-to-drag ratio C_L/C_D is the objective f_1 of the optimization: $f_1 = C_L/C_D$. The function f_1 is maximized with the constraint of providing a positive lift coefficient. The second condition is the retreating side, where airfoils are generally sought to have the greatest maximum lift coefficient. Thus a measure which privileges the lift coefficient is used, that is $f_2 = C_L^{3/2}/C_D$. Finally, the constraints on the moment coefficient used in the deterministic case (and presented in the preceding section) are still considered.

In mathematical terms, the resulting optimization problem can be stated as:

$$\begin{aligned} \text{maximize :} \quad & \mu\left(f\left(\boldsymbol{x}_s, \boldsymbol{\xi}\right)\right) \\ \text{and minimize :} \quad & \sigma^2\left(f\left(\boldsymbol{x}_s, \boldsymbol{\xi}\right)\right) \\ \text{subject to :} \quad & \mathbf{g}\left(\boldsymbol{x}_s, \boldsymbol{\xi}\right) \leq \mathbf{0} \\ \text{by changing :} \quad & \boldsymbol{x}_s, \end{aligned} \tag{5}$$

where the moment constraints are collected in vector $\mathbf{g}$. It is clear that function f is equal to f_1 for the advancing side and equal to f_2 in the retreating case. The design variables are the variables defining the shape of the airfoil, while the angle of attack is considered as one of the uncertain variables in the design problem.

For this problem, the angle of attack α and the Mach number M encountered by the two-dimensional section of the blade are considered as uncertain, because they are affected by uncertainty on the modelling of the physical parameters considered in the design stage. For instance, both aerodynamic and structural uncertainties, such as blade chord, air density, and rotor angular velocity, may affect the value of the angle of attack and Mach number. Following a probabilistic framework, the uncertain variables are modelled as uniformly distributed random variables around a nominal value. The nominal conditions are reported in Tab. 1 and the uncertainty band is set to 5% for the Mach number and the angle of attack.

The objective functions of Eq. (5) are the statistics of the performance f. These are computed by means of an uncertainty propagation technique, that is a method to propagate the uncertainty affecting the operating conditions into the quantity of interest f.

3.1 Uncertainty quantification

With regard to the method used to compute the statistics of function f, the uncertainty quantification is performed by the Polynomial Chaos (PC) expansion method [17]. Considering function $v(\boldsymbol{\xi})$ (e.g. the performance for a given design vector $v(\boldsymbol{\xi}) = f(\boldsymbol{\xi}, \overline{\boldsymbol{x}_s})$, a polynomial expansion is computed in a stochastic space spanned by a complete set of orthogonal polynomials Ψ that are functions of the random variables $\boldsymbol{\xi}$

$$v(\boldsymbol{\xi}) = \sum_{k=0}^{\infty} \beta_k \Psi_k\left(\boldsymbol{\xi}\right), \tag{6}$$

where Ψ_k are the PC orthogonal polynomials and β_k the coefficients of the expansion [17]. In practice, the series has to be truncated to a finite number of terms, which is determined from the number of uncertain variables and the order of the univariate polynomial expansion $\phi_i(\xi_i)$ from which the multivariate

Case	Objective	Constraints	Design variables
DO	$\min(C_{D,1}, C_{D,2})$	$C_L = \overline{C_L},\ C_M \leq \overline{C_M}$	$\boldsymbol{x}_s, \alpha$
RO1	$\max(\mu(f_1))$ and $\min(\sigma^2(f_1))$	$C_M \leq \overline{C_M}$	$\boldsymbol{x}_s$
RO2	$\max(\mu(f_2))$ and $\min(\sigma^2(f_2))$	$C_M \leq \overline{C_M}$	$\boldsymbol{x}_s$
DMO1	$\min(C_{D,1})$	$C_L = \overline{C_L},\ C_M \leq \overline{C_M}$	$\boldsymbol{x}_c, \alpha$
DMO2	$\min(C_{D,2})$	$C_L = \overline{C_L},\ C_M \leq \overline{C_M}$	$\boldsymbol{x}_c, \alpha$
RMO1	$\max(\mu(f_1))$ and $\min(\sigma^2(f_1))$	$C_M \leq \overline{C_M}$	$\boldsymbol{x}_c$
RMO2	$\max(\mu(f_2))$ and $\min(\sigma^2(f_2))$	$C_M \leq \overline{C_M}$	$\boldsymbol{x}_c$

Table 3: Summary of optimization problems.

polynomials $\Psi_k(\boldsymbol{\xi})$ are obtained via tensorization, i.e.

$$\Psi_k(\boldsymbol{\xi}) = \prod_i^{n_\xi} \phi_i(\xi_i).$$

The polynomial basis $\phi_i(\xi_i)$ is chosen according to the Wiener-Askey scheme to select orthogonal polynomials with respect to the probability density function p_ξ. In this work, because a uniform distribution is considered, Legendre polynomials are employed. The orthogonality property can be advantageously used to compute the PC coefficients of the expansion β_k in a non-intrusive PC framework, i.e. the so-called Non-Intrusive Spectral Projection [18]. The computation of the PC coefficients requires an integration of the polynomials, obtained by means of a quadrature formula whose quadrature points have to be evaluated with samples from the exact function $v(\boldsymbol{\xi})$. As a result the reconstruction of the statistics is based on the evaluation of the exact function for a set of samples $\boldsymbol{\xi}_k$ in the uncertain variables domain for each design vector $\overline{\boldsymbol{x}_s}$. The uncertainty-based optimization procedure is thus the combination of two loops: an outer loop given by the chosen optimizer and and an inner loop which computes the statistics for each design.

4 MORPHING CAMBER OPTIMIZATION

The morphing strategy considered in this work is a conformable camber airfoil, which changes over the period of rotation of the blade. Several technological solutions can be employed to achieve this goal: for instance, the FishBone Active Camber [4], the controllable camber presented in Ref. [2] and chiral structures as the one developed in Ref. [19]. The basic idea in the definition of a camber morphing airfoil is that the thickness distribution is held fixed, while the camber is allowed to change its shape during flight. In general, the camber line cannot be modified at any chordwise coordinate, but it is held fixed in particular areas to maintain the internal structure of the blade and to accommodate morphing mechanisms. In particular, the region close to the leading edge is fixed, where the D-shaped spar used in the helicopter blade structure is found. For the remaining part of the blade section, the camber can morph to work as a trailing-edge flap with a larger extension and continuous shape modification.

A suited parameterization is required to describe and optimize a morphing camber airfoil. The parameterization introduced in Sec. 2.1 treats separately the camber line and the thickness distribution perpendicular to the local camber line. For the morphing modification, a piecewise cubic function is used which are defined to ensure continuity up to the second order. Following an approach similar to the one presented in Ref. [20], the morphing camber line is described as follows

$$\zeta_c(\psi) = C_c(\psi)\ S_c(\psi) + \sum_{i=1}^{n_c} h_i(\psi) \qquad (7)$$

and each cubic function $h_i(\psi)$ reads

$$h_i(x) = \begin{cases} 0, & \text{if } \psi \leq \psi_{0,i} \\ a_i \frac{(x-x_{0,i})^3}{(1-x_{0,i})^3}, & \text{if } \psi > \psi_{0,i}, \end{cases}$$

where a_i are the coefficients of the cubic functions and $x_{0,i}$ are the locations of the start of the morph. The number of cubic functions n_c is equal to two in order to represent also reflex cambered airfoil and the locations of the morphs are $x_{0,1} = 0.4$ and $x_{0,2} = 0.7$. The coefficients of the cubic functions are the design variables of the morphing airfoil $\boldsymbol{x}_c = \{a_1, a_2\}$.

5 RESULTS

As presented in the previous sections, several optimization problems are performed. A summary of all the optimization cases presented in this section is

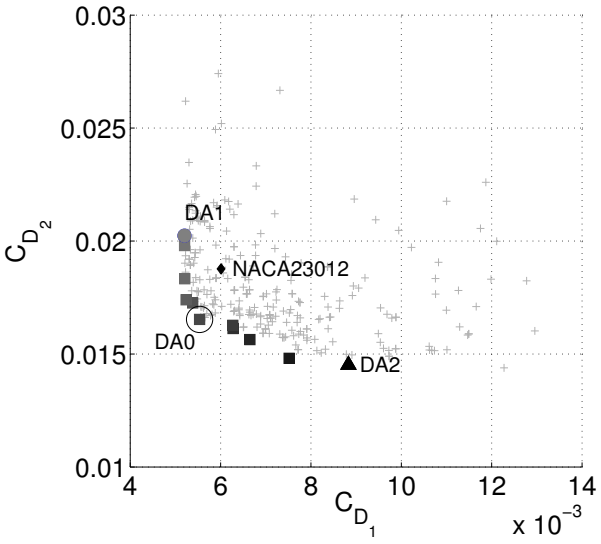

Figure 2: Pareto front of deterministic multi-point optimization (DO).

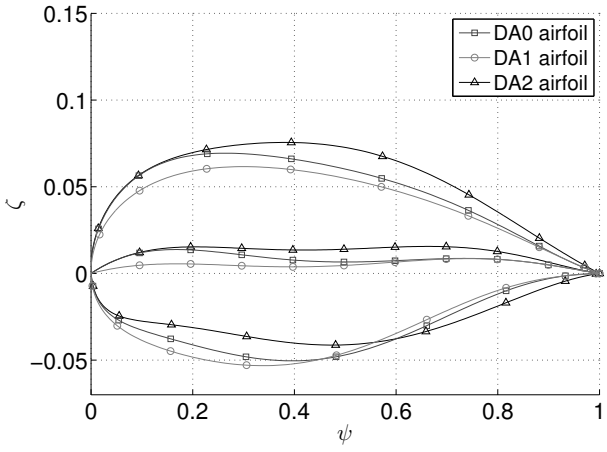

Figure 3: Optimal and trade-off airfoils of DO.

given in Tab. 3. Letters D, R and M stand for the deterministic, robust and camber morphing cases, while numbers 1 and 2 refer to advancing and retreating side, respectively.

5.1 Deterministic multi-point optimization

The first case is the optimization stated in Eq. (1), that is the minimization of the drag coefficient by changing the airfoil shape and the angle of attack. Because this is a multi-objective optimization, the result is a set of solutions representing the trade-off between the two objectives. The set is called Pareto front and it is presented in Fig. 2. In the objective space, a few airfoils are highlighted: (i) the airfoil with optimal drag coefficient in the advancing side called DA1, (ii) the airfoil with optimal drag coefficient in the retreating side called DA2, (iii) the airfoil with best trade-off called DA0, and a reference airfoil, the NACA 23012. Please note that the NACA 23012 has been reported for comparison, but it does not satisfy the lift constraint in the advancing side and therefore it does not belong to the population of the optimization.

The airfoils highlighted in the front are shown in Fig. 3. It is possible to note that the slope of the camber line at the leading edge is greater in the case of airfoil DA2 to cope with the higher angle of attack. Airfoil DA1 minimize the drag coefficient by reducing the local Mach number as presented in Fig. 4, where it is possible to note the absence of strong shock waves.

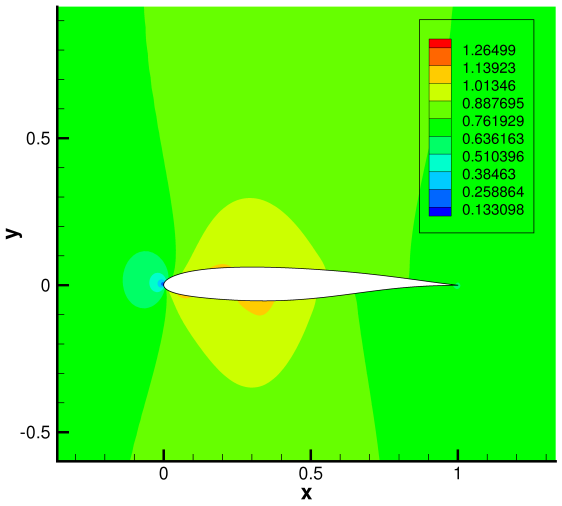

Figure 4: Mach number contour in the advancing side for airfoil DA1 of DO.

On the other hand, the local Mach number contour of airfoil DA2 (Fig. 5) presents a shock wave close to the leading edge on the lower side, which results in a drag penalty. The trade-off airfoil DA0 represents a compromise shape between the two optimal airfoils.

5.2 Robust optimization

Two different robust optimization problems are performed, the first one for the advancing side (problem RO1) and the second one for the retreating side (RO2). The Pareto front for the case of the advancing side is presented in Fig. 6 where the two objective functions are the mean value and the variance of the lift-to-drag ratio. The front presents very robust solution that however comes at the expense of poor

Airfoil	$C_{D,1}\|_{\overline{C_{L_1}}}$	$\alpha_1\|_{\overline{C_{L_1}}}$ [deg]	$\mu_{C_{D,1}}$	$\sigma^2_{C_{D,1}}$	$(\sigma/\mu)_{C_{D,1}}$
DA1	5.201e-3	-1.026	5.547e-3	4.399e-07	1.194e-1
RA1	5.209e-3	-1.510	5.369e-3	6.685e-08	4.816e-2

Table 4: Performance of the deterministic airfoil minimizing C_{D_1} (DA1) and the airfoil selected from the front of the robust optimization in the advancing side (RA1).

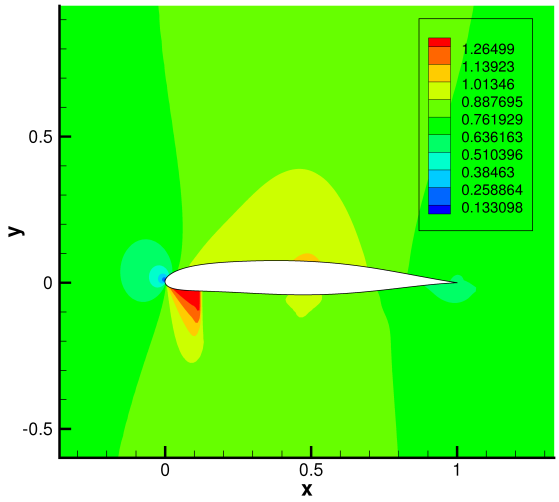

Figure 5: Mach number contour in the advancing side for airfoil DA2 of DO.

performance. In the higher part od the fron solutions with high mean value are found.

From the solutions belonging to the front, airfoil RA1 is selected, which is an airfoil that exhibits a lift coefficient equal to the target value inside the uncertainty range considered. The value of the angle of attack for which the lift coefficient of airfoil RA1 is equal to $\overline{C_{L_1}}$ is called $\alpha_1|_{\overline{C_{L_1}}}$ and it is equal to -1.51 degrees at the Mach number used for the deterministic optimization DO. As presented in Tab. 4, in this condition the drag coefficient is only slightly higher than the one provided by airfoil DA1, owing to the fact that even this airfoil does not present extended region of supersonic flow and shock waves (see Fig. 7). This means that this airfoil is capable of satisfying the trim condition with a very small drag penalty with respect to the deterministic airfoil. However, if an uncertainty band is considered around the condition ensuring trim requirement, both the mean value and the variance of the drag coefficient for airfoil RA1 are smaller than the values of airfoil DA1 (see Tab. 4). The table also presents the coefficient of variation, defined as the ration of the standard deviation σ to the mean value μ, to appreciate the dispersion with respect to the mean value.

The same analysis can be performed for the Pareto

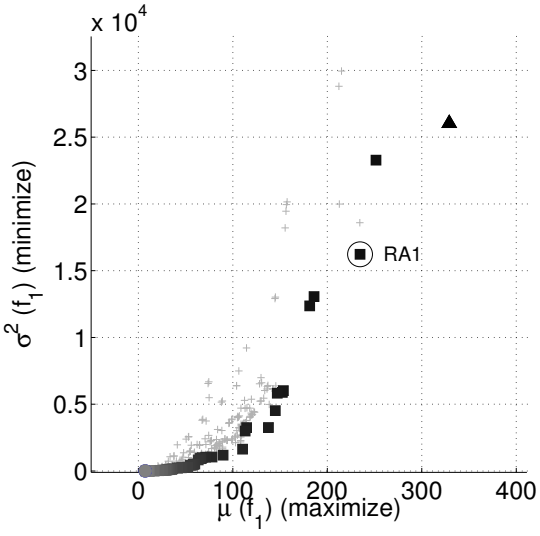

Figure 6: Pareto front of robust optimization for the advancing side (RO1).

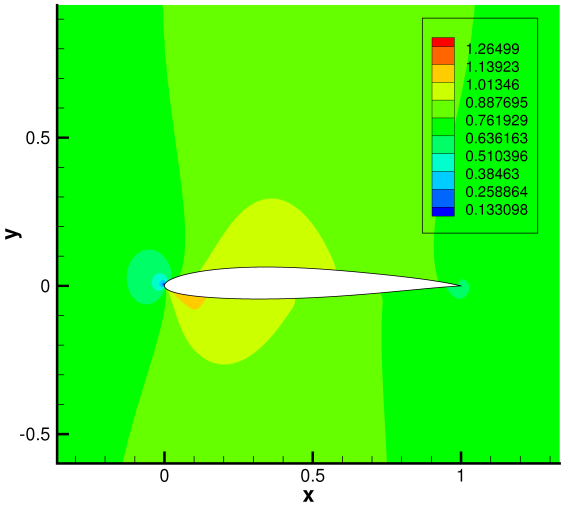

Figure 7: Mach number distribution of an optimal design selected from the robust front (advancing side) at $\alpha_1|_{\overline{C_{L_1}}} = -1.51$ deg.

front of the retreating side. Figure 8 presents the optimal set of solutions compared to the reference airfoil, the NACA 23012. In this case, every airfoil in the optimal set provides a lift coefficient that is greater than the target value $\overline{C_{L_2}}$. In future work, it may be appropriate to increase the target lift coefficient of the deterministic optimization to result in airfoils with even better performance. Thus, to select an airfoil from the front for comparison, airfoil RA2 has been chosen as a tradeoff between the two objectives. For this airfoil a lower angle of attack is needed to satisfy the trim condition, which provides also lower values of the drag coefficient (see Tab. 5). Even in this case the mean value and the variance of the drag coefficient are lower owing to a more flat distribution of the drag coefficient in the stochastic space, as shown in Fig. 9.

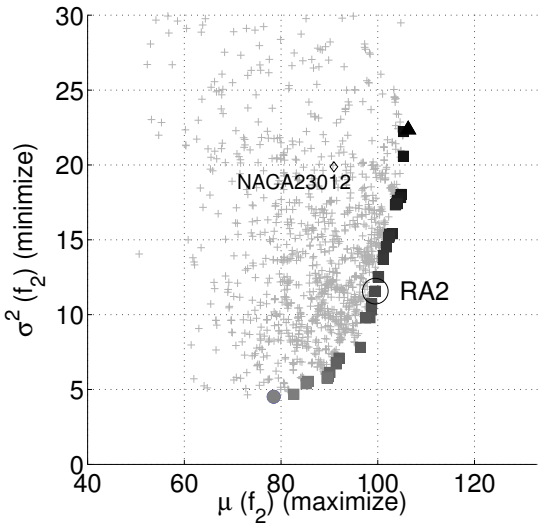

Figure 8: Pareto front of robust optimization for the retreating side (RO2).

5.3 Camber-morphing deterministic optimization

If a morphing strategy were capable to morph the helicopter blade in such a way that the airfoil blade in the advancing side was airfoil DA1 and in the retreating side the airfoil was shaped as airfoil DA2, a "perfect" morphing could be achieved with a significant gain as presented in Fig. 2. In practice, obtaining such a shape morph requires a modification of the thickness distribution which is difficult to obtain with the existing technologies. Thus, moving from airfoil DA0, i.e. the airfoil with the best tradeoff between the drag coefficient in the advancing and retreating sides, a camber modification with two cubic functions

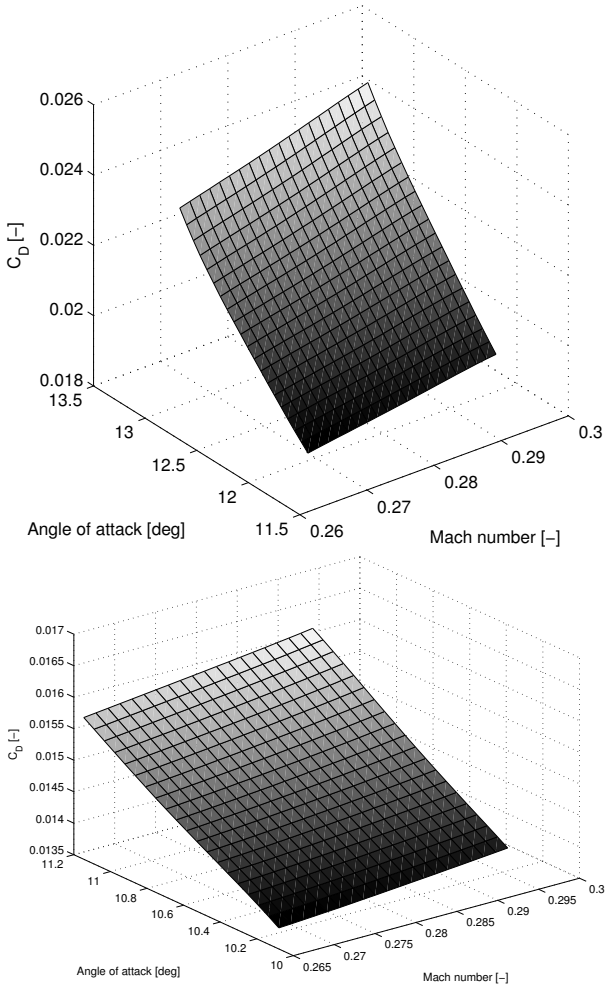

Figure 9: Drag coefficient of DA2 and RA2 in the uncertainty band around $\alpha_1|_{\overline{C_{L_1}}}$.

Airfoil	$C_{D,2}\|_{\overline{C_{L_2}}}$	$\alpha_1\|_{\overline{C_{L_2}}}$ [deg]	$\mu_{C_{D,2}}$	$\sigma^2_{C_{D,2}}$	$(\sigma/\mu)_{C_{D,2}}$
DA2	0.02047	12.433	0.02154	2.176e-06	0.0684
RA2	0.01481	10.657	0.01484	3.383e-07	0.0392

Table 5: Performance of the deterministic airfoil minimizing C_{D_2} (DA2) and the airfoil selected from the front of the robust optimization in the retreating side (RA2).

is considered and computed by means of different optimization problems. The first set of optimization is the deterministic minimization of the lift coefficient obtained by acting on the design variables $\boldsymbol{x}_c$ and the angle of attach α. The second set of optimization is based on two robust optimization problems, each performed in each side of the blade.

In the former case, two separate optimization problems are performed to rapidly converge on the interesting cases, namely the extreme airfoils of the front. The resulting airfoils share the same thickness distribution of airfoil DA0, but the drag coefficient is lower in the advancing and retreating side thanks to the camber morph. The airfoils are presented in Fig. 10, while the gain with respect to airfoil DA0 are reported in Tab. 6. The gain is obtained by changing the final part of the shape and it is not so pronounced, probably due to the fact that fixing the thickness poses an excessive constraint to the optimization problem. In future work, an optimization with the complete set of variables ($\boldsymbol{x}_s$, $alpha$ and $\boldsymbol{x}_c$) will be considered.

In the second set, two robust optimization problems are performed. Thus, the results are two Pareto fronts, similarly to the case presented in the preceding section. From each optimal set an airfoil is selected with the same criterion used for the non-morphing case. Indeed, the chosen airfoil represents the best trade-off between the mean value and the variance, but also guarantees the satisfaction of the target lift coefficient within the considered uncertainty band. The airfoils coming from the robust optimization for the advancing side is labelled RMA1 and RMA2 is used for the retreating side. The mean values and the variance obtained with an uncertainty band around the condition providing trim satisfaction are compared in Tabs. 7 and 8. It is possible to note that the robust airfoils present lower values of the variance with a small drag penalty of the drag coefficient in the nominal condition. Further analysis will be required to completely assess the trend shown in this preliminary comparison.

Airfoil	$C_{D,2}\|_{\overline{C_{L_2}}}$	$C_{D,2}\|_{\overline{C_{L_2}}}$	Percentual gain
DMA1	0.005504	–	1%
DMA2	–	0.01593	4%

Table 6: Performance of the deterministic best C_{D_1} (DMA1) and deterministic best C_{D_2} (DMA2) with respect to the baseline airfoil DA0.

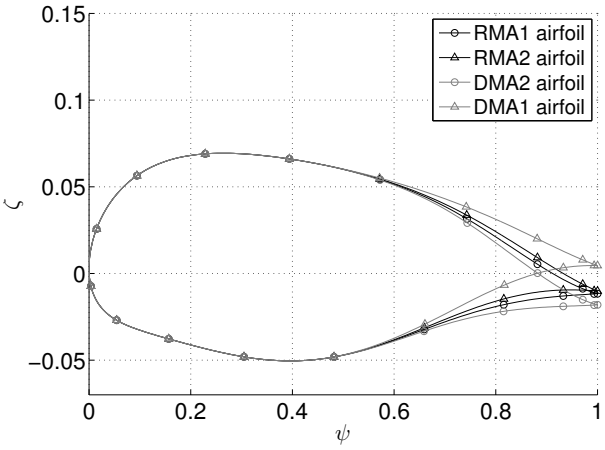

Figure 10: Optimal airfoil with camber morphing: deterministic best C_{D_1} (DMA1), deterministic best C_{D_2} (DMA2), selected airfoil from robust Pareto in the advancing side (RMA1) and selected airfoil from robust Pareto in the retreating side (RMA2).

6 CONCLUSIONS

A robust approach is presented for the optimization of morphing airfoils for helicopter rotor blades. The robust approach enables to limit the variance of the performance when considering the uncertainty affecting the operating conditions at the design stage. The robust strategy founds airfoils that can satisfy the lift coefficient constraint necessary for trim requirement, suffer only of a low drag penalty in the nominal condition, but provides better variance of the drag coefficient and mean value in one of the cases. With regard to the morphing strategy, a camber morphing is tested to improve an optimal baseline design with technological constraints. Further analysis is necessary to improve the preliminary estimates on the gain

Airfoil	$C_{D_1}\|_{\overline{C_{L_1}}}$	$\alpha_2\|_{\overline{C_{L_1}}}$ [deg]	$\mu_{C_{D_1}}$	$\sigma^2_{C_{D_1}}$	$(\sigma/\mu)_{C_{D_1}}$
DMA1	5.484e-3	-1.14	7.075e-03	4.063732e-06	0.285
RMA1	6.393e-3	-1.28	6.258e-03	3.574504e-06	0.267

Table 7: Performance of the morphing camber airfoil minimizing C_{D_1} (DMA1) and the airfoil selected from the front of the robust optimization in the advancing side (RMA1).

Airfoil	$C_{D_2}\|_{\overline{C_{L_2}}}$	$\alpha_2\|_{\overline{C_{L_2}}}$ [deg]	$\mu_{C_{D_2}}$	$\sigma^2_{C_{D_2}}$	$(\sigma/\mu)_{C_{D_2}}$
DMA2	0.01593	10.01	1.609e-02	3.431e-06	0.1151
RMA2	0.01697	11.37	1.694e-02	5.207e-07	0.0426

Table 8: Performance of the morphing camber airfoil minimizing C_{D_2} (DMA2) and the airfoil selected from the front of the robust optimization in the retreating side (RMA2).

of camber morphing airfoils. Future work will also address the problem of validating the results with unsteady CFD computations to better appreciate the quality of the information that may come from multipoint approaches such as the one presented in this paper.

References

[1] Barbarino, S., Bilgen, O., Ajaj, R. M., Friswell, M. I., and Inman, D. J., "A Review of Morphing Aircraft," *Journal of Intelligent Material Systems and Structures*, Vol. 22, No. 9, Aug. 2011, pp. 823–877.

[2] Gandhi, F., Frecker, M., and Nissly, A., "Design Optimization of a Controllable Camber Rotor Airfoil," *AIAA Journal*, Vol. 46, No. 1, Jan. 2008, pp. 142–153.

[3] Kerho, M. F., "Adaptive Airfoil Dynamic Stall Control," *Journal of Aircraft*, Vol. 44, No. 4, July 2007, pp. 1350–1360.

[4] Murugan, M. S., Woods, B. K. S., and Friswell, M. I., "Morphing helicopter rotor blade with curvilinear fiber composites," *38th European Rotorcraft Forum*, 2012.

[5] Siva, C., Murugan, M. S., and Ganguli, R., "Uncertainty Quantification in Helicopter Performance Using Monte Carlo Simulations," *Journal of Aircraft*, Vol. 48, No. 5, Sept. 2011, pp. 1503–1511.

[6] Murugan, S., Chowdhury, R., Adhikari, S., and Friswell, M., "Helicopter aeroelastic analysis with spatially uncertain rotor blade properties," *Aerospace Science and Technology*, Vol. 16, No. 1, 2012, pp. 29 – 39.

[7] Fusi, F., Guardone, A., Quaranta, G., and Congedo, P. M., "Multi-fidelity physics-based method for robust optimization with application to a hovering rotor airfoil," *AIAA Journal*, 2015.

[8] Johnson, W., *Rotorcraft Aeromechanics*, Cambridge University Press, New York, 2013.

[9] Massaro, A. and Benini, E., "Multi-Objective Optimization of Helicopter Airfoils Using Surrogate-Assisted Memetic Algorithms," *Journal of Aircraft*, Vol. 49, No. 2, March 2012, pp. 375–383.

[10] Morris, A., Allen, C., and Rendall, T., "Aerodynamic Optimisation of Hovering Helicopter Rotors using Efficient and Flexible Shape Parameterisation," *26th AIAA Applied Aerodynamics Conference*, 2008.

[11] Fanjoy, D. and Crossley, W. A., "Aerodynamic Shape Design for Rotor Airfoils via Genetic Algorithm," , pp. 263–270.

[12] Kulfan, B. M. and Bussoletti, J. E., "Fundamental Parametric Geometry Representation for Aircraft Component Shapes," *11th AIAA/ISSMO Multidisciplinary Analysis and Optimization Conference*, 2006.

[13] Palacios, F., , Colonno, M. R., Aranake, A. C., Campos, A., Copeland, S. R., Economon, T. D., Lonkar, A., Lukaczyk, T. W., Taylor, T. W. R., and Alonso, J. J., "Stanford University Unstructured (SU2): An open-source integrated computational environment for multi-physics simulation and design," *51st AIAA Aerospace Sciences Meeting including the New Horizons Forum and Aerospace Exposition*, 2013.

[14] Palacios, F., Economon, T. D., Aranake, A. C., Copeland, S. R., Lonkar, A. K., Lukaczyk, T. W., Manosalvas, D. E., Naik, K. R., Padron, A. S., Tracey, B., Variyar, A., and Alonso, J. J., "Stanford University Unstructured (SU2): Open-source Analysis and Design Technology for Turbulent Flows," *52nd Aerospace Sciences Meeting*, 2014.

[15] Kenway, G. and Martins, J. R. R. A., "Multipoint High-Fidelity Aerostructural Optimization of a Transport Aircraft Configuration," *Journal of Aircraft*, Vol. 51, No. 1, 2014, pp. 144–160.

[16] Drela, M., "XFOIL: An Analysis and Design System for Low Reynolds Number Airfoils." *Conference on Low Reynolds Number Airfoil Aerodynamics*, 1989.

[17] Xiu, D. and Karniadakis, G. E., "The Wiener–Askey Polynomial Chaos for Stochastic Differential

Equations," *SIAM Journal on Scientific Computing*, Vol. 24, No. 2, Jan. 2002, pp. 619–644.

[18] Congedo, P. M., Corre, C., and Martinez, J.-M., "Shape optimization of an airfoil in a BZT flow with multiple-source uncertainties," *Computer Methods in Applied Mechanics and Engineering*, Vol. 200, No. 1-4, Aug. 2011, pp. 216–232.

[19] Airoldi, A., Crespi, M., Quaranta, G., and Sala, G., "Design of a Morphing Airfoil with Composite Chiral Structure," *Journal of Aircraft*, Vol. 49, No. 4, July 2012, pp. 1008–1019.

[20] Fincham, J. and Friswell, M., "Aerodynamic optimisation of a camber morphing aerofoil," *Aerospace Science and Technology*, Vol. 43, 2015, pp. 245 – 255.